Supporting Information

Resistive Switching Memory Effects of NiO Nanowire/Metal Junctions

Keisuke Oka[1], Takeshi Yanagida[1,2]*, Kazuki Nagashima[1], Tomoji Kawai[1,3]*,

Jin-Soo Kim[3] and Bae Ho Park[3]

1 Institute of Scientific and Industrial Research, Osaka University, 8-1 Mihogaoka Ibaraki, Osaka, 567-0047, Japan

2 PRESTO, Japan Science and Technology Agency, 4-1-8 Honcho Kawaguchi, Saitama, 332-0012, Japan

3 Division of Quantum Phases & Devices, Department of Physics, Konkuk University, Seoul 143-701, Korea

* E-mail: yanagi32@sanken.osaka -u.ac.jp, kawai@sanken.osaka-u.ac.jp.

1. Experimental Details

Fabrication of NiO nanowires. NiO nanowires were fabricated as core/shell heterostructured nanowires by using in-situ heterostructured oxide nanowire formation technique. The ideal crystal combination between NiO and MgO, including the same crystal structures (rock-salt) and the small lattice mismatch (0.7%), and the use of the in-situ heterointerface formation technique are essential to fabricate the well-defined single crystalline NiO heterostructured nanowires. NiO shell layers were deposited onto MgO core nanowires without atmospheric exposures. The MgO core nanowires were grown on MgO (100) single crystal substrate by Au-catalyst assisted vapor-liquid-solid (VLS) growth utilizing a pulsed laser deposition (PLD). ArF excimer laser (Lamda-Physik COMPex 102, λ=193nm) was used for the laser ablation. Au catalyst thin film with the thickness of 0.7nm was deposited on the substrate. MgO single crystal was used as a source of Mg species. The laser energy, the repetition rate, and the distance between the substrate and the target were set to be 40mJ, 10Hz, and 30mm, respectively. Oxygen and argon mixed gas was introduced into the chamber by controlling the ambient total pressure of 10Pa with the flux ratio of oxygen and argon (1:1000). The Au-coated single crystal substrate was preheated at 750ºC for 10min. After 5 hours of the nanowire growth, the samples were cooled down to room temperature (RT). The average diameter and length of the MgO nanowires were controlled to be 10nm and 5μm, respectively. After MgO core nanowire growth, MgO/NiO core/shell nanowires were synthesized by using in-situ nanowire template method. NiO shell layer was formed onto MgO core nanowires by using PLD without atmospheric exposure. NiO pellet (99.999% pure) was used as the target. For the shell layer formation, the background pressure of the chamber was less than 5×10^{-6}Pa. The shell layer formation was performed under 300 ºC and 10^{-3}Pa of the oxygen pressure (oxygen gas: 99.9999% pure). The deposition rate for NiO shell layer growth was ~0.4 Å/min. The laser energy, the repetition rate, and the distance between the substrate and the target source were set to 40mJ, 10Hz, and 45mm, respectively.

Sample Characterizations. To characterize the morphology, the diameter, the microstructures, the crystal structure, and the composition of fabricated nanowires, a field emission scanning electron microscopy (FESEM, Hitachi S-4300) at an accelerating voltage of 30kV and a high resolution transmission electron microscopy (HRTEM, JEOL JEM-3000F) at an accelerating voltage of 300kV coupled with energy dispersive spectroscopy (EDS) were used.

Fabrication of Metal/Nanowire/Metal Junctions. NiO nanowire/metal junctions were fabricated by combining photolithography and electron-beam (EB) lithography processes. First, as-grown NiO nanowires on the substrate were sonicated and dispersed in 2-propanol. The frequency and the sonication time were 28kHz and 20min, respectively. Then the dispersed NiO nanowires were transferred onto degenerately doped *n*-type silicon substrate capped with a 300 nm SiO_2 layer. Before transferring the nanowires onto SiO_2/Si substrate, the macro-electrodes for contacting of electrical probes were fabricated by photolithography. EB lithography was performed after fabricating the macro-electrodes by photolithography. After EB lithography patterning, Pt/Au (20nm/100nm) as nano-gap electrodes were deposited to contact electrically between the macro-electrodes and the nanowires, as shown in Figure S1(a). The use of Pt electrode is important to avoid an interfacial oxidized layer for reliable junctions. Figure S1 (b) shows the SEM image of the junction with the nano-gap spacing controlled to be about 300nm in this work. Electrical measurements were performed by using a semiconductor analyzer (Keithley 4200SCS) in atmospheric air at RT, as shown in Figure S1(c). In this system, it is possible to vary the atmosphere gas. Data retention measurements were performed in the condition (~10^{-1}Pa and RT). The resistances of LRS were measured at 2 V.

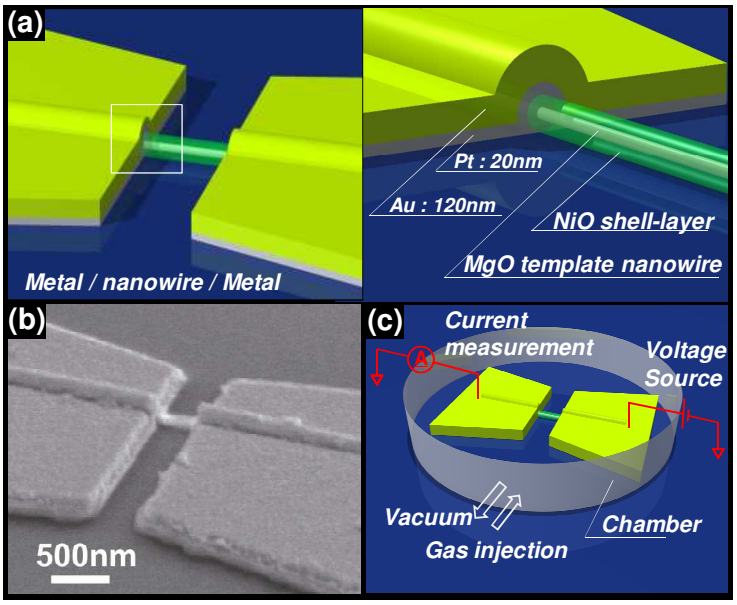

Figure S1. (a) Schematic image of junction composed of NiO nanowire and Pt/Au metal electrode, (b) FESEM image of NiO nanowire/Pt junction, (c) Measurement system to investigate the atmosphere gas dependence on the transport properties.

2. Endurance Data of NiO Nanowire/Pt Junction

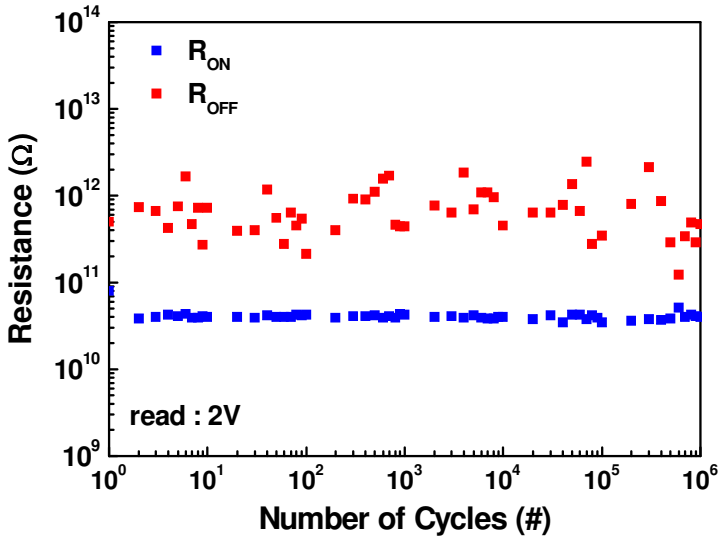

Figure S2. Endurance data of fabricated NiO nanowire/Pt junction.

Figure S2 shows the endurance data of fabricated NiO nanowire/Pt junction. It can be seen that the fabricated junction exhibited highly stable RS properties with the endurance at least up to 10^6. This is in

contrast with the case when using C-AFM, in which the endurance was confirmed only for several times due to the instability of conductive tip. Thus the present NiO nanowire/Pt metal junctions are much more superior to C-AFM in terms of the methodological stability. The feasibility of such stable junctions is due to the use of well-defined metal/nanowire contact via Pt layer. Note that the use of Pt layer is crucial to realize such stable metal/oxide nanowire junctions.

3. Compliance Current Dependence on Resistive Switching of NiO nanowire/Pt Junctions

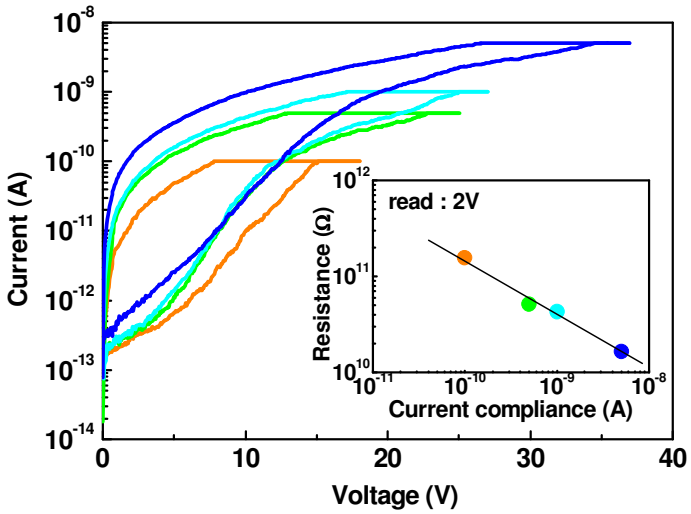

Figure S3. Compliance current dependence on RS of NiO nanowire/Pt Junctions, measured in air. The inset shows the resistance value of low resistance state (LRS) when varying the compliance current.

Figure S3 shows the compliance current dependence on RS of NiO nanowire/Pt Junctions. It can be seen that varying the compliance current value resulted in the variation of LRS resistance. More importantly, there was a systematic relationship between the compliance current and the LRS resistance, indicating the multistate memory effects. The inset shows the compliance current dependence on the resistance value of low resistance state (LRS). The resistance value of LRS was measured at 2 V. LRS resistance systematically decreased with increasing the compliance current. The LRS/high resistance state (HRS) resistance ratio increased when increasing the compliance current. These results highlight

the feasibility of the present NiO nanowire/metal junctions for oxide nanowire-based multistate non-volatile RS memory devices. Although the switching polarity of the present junctions differs from that of C-AFM, the polarity of the present junction is arbitrary since the present junction is comprised of symmetric two electrodes.

4. RS Properties of Metal/Epitaxial NiO Film/Metal (MIM) Sandwich Devices

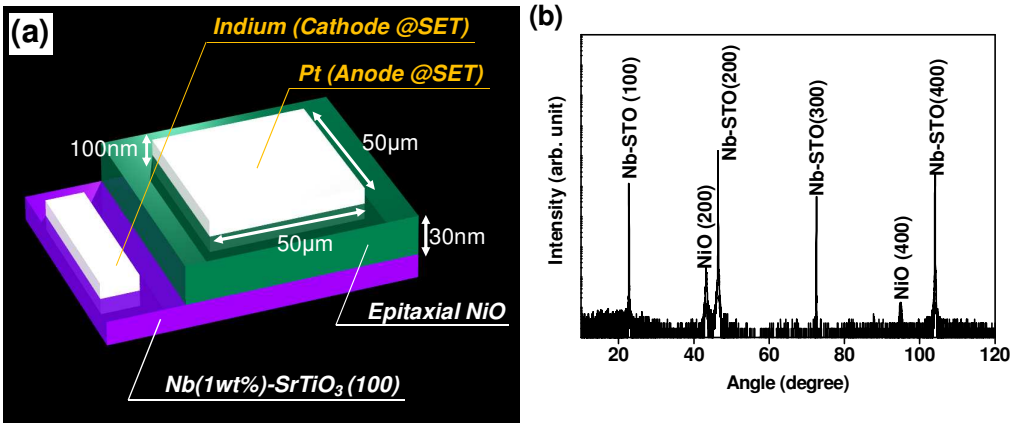

Figure S4. (a) Schematic image of metal/epitaxial NiO thin film/metal (MIM) sandwich RS device structure. (b) XRD data of fabricated MIM structure.

Figure S4 (a) shows the schematic image of fabricated metal/NiO film/metal sandwich RS device structure. NiO films were deposited onto Nb(1wt%) doped $SrTiO_3$ single crystal substrate (metallic) by using PLD. For the NiO film formations, the temperature, the oxygen partial pressure, the target, the laser power, the laser frequency and the deposition rate were 300ºC, 10^{-3}Pa, NiO pellet, 40mJ, 10Hz and 0.17nm/min, respectively. The Pt top metal electrode was deposited onto NiO films by RF sputtering. The epitaxial growth of NiO film on Nb(1wt%) doped $SrTiO_3$ single crystal substrate was confirmed by XRD as seen in Figure S4 (b).

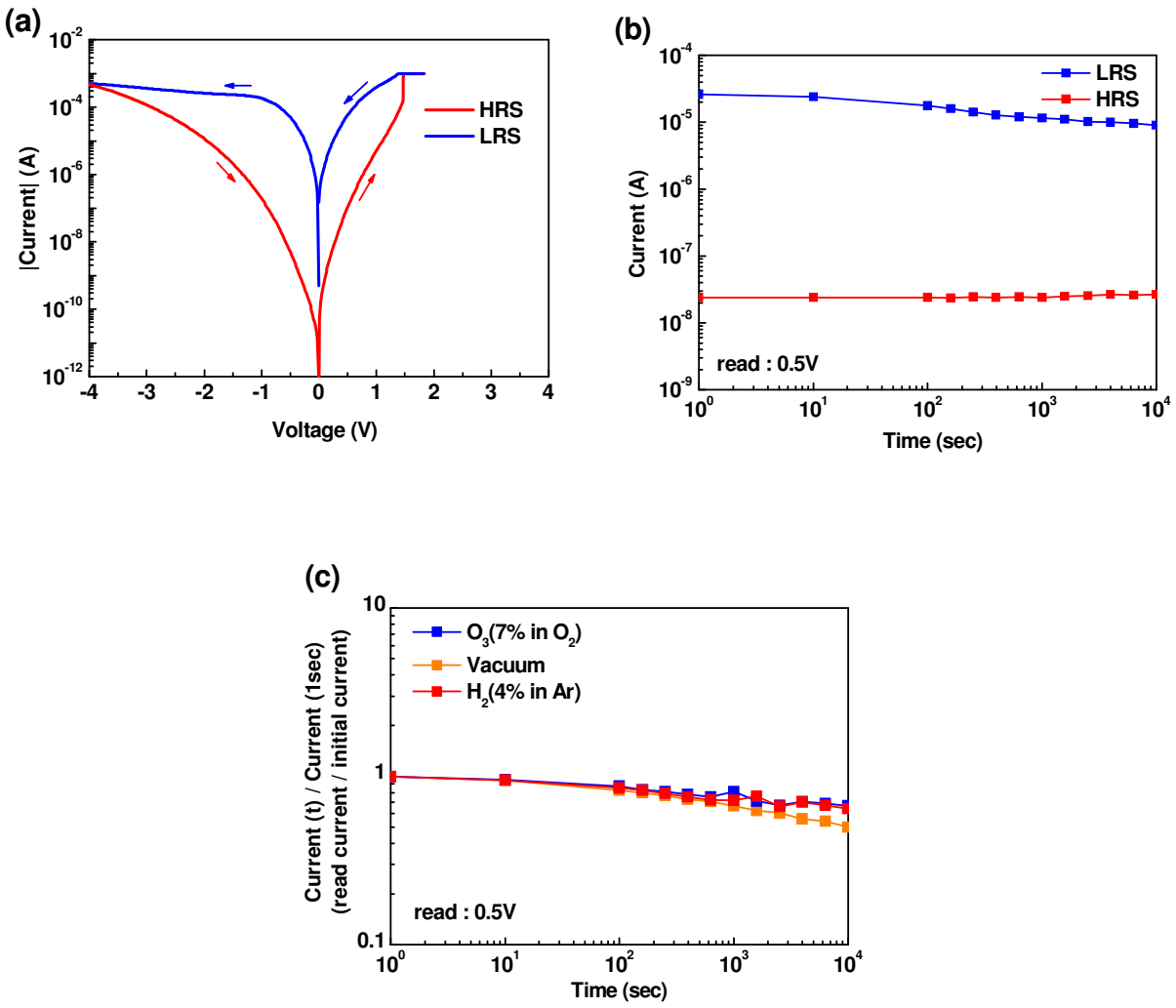

Figure S5. (a) *I-V* data of fabricated MIM sandwich RS device. (b) Retention data of LRS and HRS in fabricated MIM RS devices. (c) Atmosphere gas dependence of MIM sandwich structures.

Figure S5 (a) shows the typical *I-V* data of fabricated MIM sandwich structures. The bipolar RS properties were observed. The transition from HRS to LRS (SET process) occurred at the positive electric field, whereas the transition from LRS to HRS (RESET process) occurred at the negative electric field. The switching electric field at SET differs from at RESET. This might be due to Schottky barrier between NiO and Nb(1wt%) doped $SrTiO_3$. Both LRS and HRS were maintained at least over 10^4 sec, as shown in Figure S5 (b), indicating the non-volatile memory effects. The presence of bipolar RS in NiO film based MIM sandwich structures is consistent with the results of NiO nanowire/metal junctions. We further investigated the atmosphere gas dependence of RS properties in the MIM structure.

Figure S5 (c) shows the atmosphere gas dependence of LRS retention data. As can be seen, LRS current was found to be insensitive to the variation of atmosphere gases. In fact, the insensitivity differs from the trend of NiO nanowire/metal junctions, although both nanowire junctions and MIM structures exhibited the same bipolar RS. This is due to the difference of oxygen source for redox events. The bipolar resistive switching on metal/oxide/metal sandwich structures has been previously reported, where the initial resistance was typically a low resistance state. This behavior has been interpreted in terms of Schottky diodes with the motions of oxygen vacancies by creating the depletion layer at the interface. However, in our results, the initial state of NiO nanowire junctions was a high resistance state. If the resistive switching is caused only by changing the depletion layer, the resistance should increase from the initial resistance value by the electric field, which is obviously inconsistent with our experimental results. Although Schottky effect should exist, the effect alone can not explain our experimental trends with symmetric Pt contacts.

5. Effect of Passivation Layer on RS Properties of NiO Nanowire/Pt Junctions

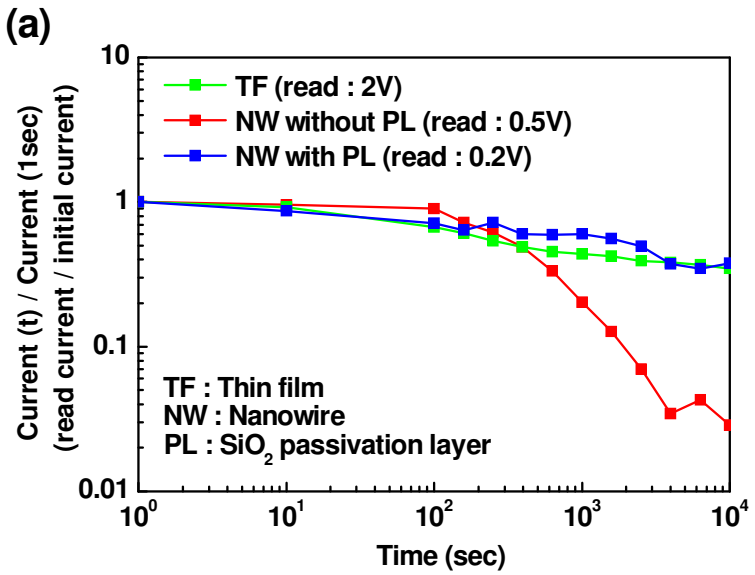

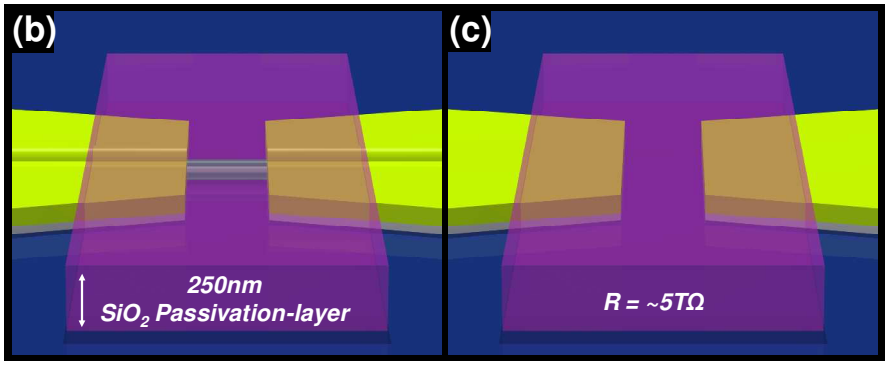

Figure S6. (a) Effect of SiO_2 passivation layer on RS properties of NiO nanowire/Pt junctions. The retention data of LRS in air were shown. For comparison, the data of thin film MIM sandwich device and nanowire junction without passivation layer were shown. (b) and (c) show the schematic images of the fabricated structures; amorphous SiO_2 passivation layer on nanowire/metal junctions.

Figure S6 (a) shows the effect of passivation layer on RS endurance data of NiO nanowire/Pt junctions. SiO_2 passivation layer was deposited onto nanowire/metal junctions by sputtering-Figure S6 (a) and (b). We confirmed the absence of RS events without nanowires by measuring the gap electrodes with SiO_2 passivation layer, where the resistance was over 5TΩ. In Figure S6 (a), the LRS current data of NiO nanowire/Pt junction without passivation layer, NiO nanowire/Pt junction with passivation layer and NiO film based MIM structure were shown. It can be seen that the presence of passivation layer strongly enhanced the retention data of NiO nanowire/Pt junction, which was comparable with MIM structure data.

Complete Ref. 3

(3) Ahn, S.; Lee, M.; Park, Y.; Kang, B. S.; Lee, C. B.; Kim, K. H.; Seo, S.; Suh, D.; Kim, D.; Hur, D.; Xianyu, W.; Stefanovich, G.; Yin, H.; Yoo, I.; Lee, J.; Park, J.; Baek, I.; Park, B. H. *Adv. Mater.* **2008**, 20, 924.